

# Linköping University Post Print

## A bulk plasma model for dc and HiPIMS magnetrons

N Brenning, I Axnas, M A Raadu, Daniel Lundin and Ulf Helmersson

N.B.: When citing this work, cite the original article.

Original Publication:

N Brenning, I Axnas, M A Raadu, Daniel Lundin and Ulf Helmersson, A bulk plasma model for dc and HiPIMS magnetrons, 2008, PLASMA SOURCES SCIENCE and TECHNOLOGY, (17), 4, 045009.

<http://dx.doi.org/10.1088/0963-0252/17/4/045009>

Copyright: Iop Publishing

<http://www.iop.org/>

Postprint available at: Linköping University Electronic Press

<http://urn.kb.se/resolve?urn=urn:nbn:se:liu:diva-16092>

# A bulk plasma model for dc and HIPIMS magnetrons

N Brenning<sup>1</sup>, I Axnäs<sup>1</sup>, M A Raadu<sup>1</sup>, D Lundin<sup>2</sup>, and U Helmersson<sup>2</sup>

<sup>1</sup>Division of Space and Plasma Physics, School of Electrical Engineering,, Royal Institute of Technology, SE-100 44 Stockholm, Sweden

<sup>2</sup>Plasma & Coating Physics Division, IFM-Material Physics, Linköping University, SE-581 83 Linköping, Sweden

E-mail: nils.brenning@ee.kth.se

## Abstract

A plasma discharge model has been developed for the bulk plasma (also called the extended presheath) in sputtering magnetrons. It can be used both for high power impulse magnetron sputtering (HIPIMS) and conventional dc sputtering magnetrons. Demonstration calculations are made for the parameters of the HIPIMS sputtering magnetron at Linköping University (LiU), and also bench-marked against results in the literature on dc magnetrons. New insight is obtained regarding the structure and time development of the currents, the electric fields, and the potential profiles. The transverse resistivity  $\eta_{\perp}$  has been identified as having fundamental importance both for the potentials profiles and for the motion of ionized target material through the bulk plasma. New findings are that in the HIPIMS mode, as a consequence of a high value of  $\eta_{\perp}$ , (1) there can be an electric field reversal that in our case extends 0.01-0.04 m from the target, (2) the electric field in the bulk plasma is typically an order of magnitude weaker than in dc magnetrons, (3) in the region of electric field reversal the azimuthal current is diamagnetic in nature, *i.e.*, mainly driven by the electron pressure gradient, and actually somewhat reduced by the electron Hall current which here has a reversed direction, and (4) the azimuthal current above the racetrack can, through resistive friction, significantly influence the motion of the ionized fraction of the sputtered material and deflect it sideways, away from the target and towards the walls of the magnetron.

PACS codes: 52.25.Fi, 52.50.Dg, 52.77.Dq

Submitted to Plasma Sources Sci. Technol.

## 1. Introduction

Magnetron sputtering is an important industrial process for many applications ranging from deposition of hard coatings to deposition of functional coatings for electronic applications. One of the most promising such techniques is high power impulse magnetron sputtering (HIPIMS), which was introduced by Kouznetsov *et al.* [1] in 1999 and recently reviewed by Helmersson *et al.* [2]. By using high power to the magnetron, supplied in short very intense pulses, one can increase the plasma density from  $10^{15} \text{ m}^{-3}$  for conventional dc magnetron sputtering to above  $10^{19} \text{ m}^{-3}$  for HIPIMS [3]. Generating a high plasma density increases the probability for ionizing collisions, and thereby produces a large fraction of ionization of the sputtering gas as well as the sputtered material, the latter 30-90 % depending on material and discharge parameters [4].

There are several important differences between HIPIMS and conventional dc magnetron sputtering. Most serious is a reduction in the deposition yield, down to typically 30% of that of a dc magnetron at the same average power [2]. Two possible reasons for this reduction are found in the bulk plasma. First, it might be a direct consequence of the high degree of ionization: Bradley *et al* [5] have found that in dc magnetrons the bulk plasma is associated with electric fields directed towards the target, and with a net potential difference substantially higher than the typical energy 5 eV of a sputtered neutral atom. If both the potential pattern and the particle energies were the same in the HIPIMS mode, this would attract back almost all of the ionized sputtered material. Furthermore, the azimuthal current above the racetrack exerts a volume force on the ions through resistive friction that might deflect the target metal  $M^+$  ions away from the substrate, sideways towards the walls. This will be described below.

The present work is part of a study of HIPIMS magnetrons by a combination of experimental studies [4,6,7,8] with theoretical models. In a separate paper [9] we model the ionization region above the racetrack, while the present paper deals with the bulk plasma volume which we define as the space on the substrate side of the ionization region. The results are one Ionization Region Model (IRM) in [9] and one Bulk Plasma Model (BPM) presented here. Figure 1 shows the magnetic topology of the HIPIMS magnetron at Linköping University (LiU), and the geometrical separation into one volume for the IRM and one for the BPM model. The IRM model [9] is a time dependent global (zero-dimensional) model that solves the coupled differential equations for ion, electron, and neutral species production and loss in the ionization region above the racetrack defined by  $z_1 < z < z_2$  and  $r_{c1} < r_c < r_{c2}$ . The Bulk Plasma Model, BPM, is 2-dimensional model ( $z$

A bulk plasma model for magnetrons

and cylindrical radius  $r_c$ , assuming rotational symmetry) that solves for  $n_e(z, r_c, t)$ ,  $T_e(z, r_c, t)$ ,  $\mathbf{E}(z, r_c, t)$ ,  $U(z, r_c, t)$ ,  $\mathbf{J}_D(z, r_c, t)$ , and  $\mathbf{J}_\phi(z, r_c, t)$  in the bulk plasma outside the ionization region. The IRM and BPM models can either be used independently or coupled together by the boundary conditions of a common discharge current  $I_D(t)$  and, at the geometrical interface  $(z_2, r_c)$ , common plasma density  $n_e(t)$  and electron temperature  $T_e(t)$ .

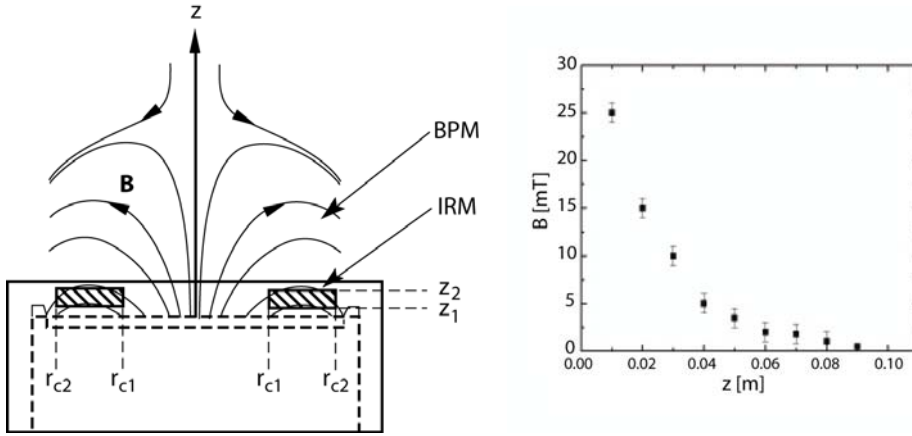


Figure 1. Left: The magnetic field topology of the HIPIMS magnetron at Linköping University (LiU), and the volumes covered by the bulk plasma model (BPM) reported here and the ionization region model (IRM) of [9]. Right: The magnetic field strength over the racetrack centre (From [6]).

The prime targets for modeling here, where we focus on the bulk plasma, are the electric fields, potentials, and current densities. The findings are partly positive, partly negative for the deposition yield: the bulk plasma electric field towards the target that needs to be maintained by the external circuit in order to drive the discharge current are an order of magnitude weaker in the HIPIMS mode, and it might even reverse polarity in the vicinity of the ionization region. Both these effects would help the motion of the ions towards the substrate. However, there can be a substantial ion acceleration in the azimuthal direction which is only significant when magnetrons are run in the HIPIMS mode. The force on the ions is due to electron-ion friction and is proportional to the product of the anomalous transverse resistivity  $\eta_\perp$  and the azimuthal current density  $\mathbf{J}_\phi$  above the racetrack (usually called the Hall current).

## 2. The Bulk Plasma Model, BPM

The bulk plasma model is designed flexibly with an input file for the parameters defining the discharge one wants to model: the magnetic field topology, the cross- $\mathbf{B}$  resistivity function, the discharge current  $I_D(t)$  and voltage  $U_D(t)$ , etc. These can be either known parameters from a performed experiment, or hypothetical parameters to test the effect of untried parameter combinations. The model then calculates, as function of time and space, the discharge parameters that remained undetermined in the input file: the electron density and temperature, the current densities, the electric field strength, etc.

For demonstration and benchmarking purposes we have taken the magnetic field of the HIPIMS magnetrons at LiU in Figure 1. The magnetic field  $\mathbf{B}(z, r_c)$  is calculated from an array of surface dipole strengths located where the real magnets have their surface, 0.009 m below the target surface. This reproduces the real field, as measured in [6], within a few percent in the whole discharge volume and is put in a  $\mathbf{B}(z, r_c)$  array of  $500 \times 500$  grid points. For the discharge current  $I_D(t)$  and the input values of  $n_e(t)$  and  $T_e(t)$  at  $(z = z_2, r_c = r_{rc})$  we have run three different cases with parameters as listed in Table. 1: experimental data from the 300 kW discharge by Böhlmark *et al* [6], experimental data from the 50 kW discharge by Lundin *et al* [7] (shown in Figure 2), and calculated data from the IRM model [9] run for parameters close to [7]. For the variations of  $n_e(z)$  and  $T_e(z)$  in the  $z$ -direction we have used exponential fits to the experimental data in Figure 2 and obtained the scale lengths 0.0195 m and 0.0172 m, respectively.

The calculation procedure in the model is described in Appendix A. The Generalized Ohm's Law [10] is split up into two equations, one for the pressure-driven part  $\mathbf{J}_{\nabla p_e}$  of the current density across  $\mathbf{B}$ ,

$$\eta_{\perp} \mathbf{J}_{\nabla p_e} + \frac{\mathbf{J}_{\nabla p_e} \times \mathbf{B}}{en_e} = \frac{\nabla p_e}{en_e}, \quad (2.1)$$

and one for the part  $\mathbf{J}_E$  of the current density across  $\mathbf{B}$  that is driven by the electric field,

$$\eta_{\perp} \mathbf{J}_E + \frac{\mathbf{J}_E \times \mathbf{B}}{en_e} = \mathbf{E}. \quad (2.2)$$

These are then solved in the bulk plasma space for each time step. In the model runs of the following section the calculated quantities are the current densities  $\mathbf{J}_D(z, r_c, t)$  and  $\mathbf{J}_{\phi}(z, r_c, t)$ , the electric field vector  $\mathbf{E}(z, r_c, t)$ , and the potential  $U(z, r_c, t)$ .

Table 1. The input parameters used for the three model runs.

Input file → Taken from →	Model run 1 Exp. Lundin [7]	Model run 2 IRM model [9]	Model run 3 Exp. Böhlmark [6]
B field	As in Figure 1	As in Figure 1	As in Figure 1
$r_{c1}, r_{c2}, z_1, z_2$ (mm)	20, 70, 2, 12	20, 70, 2, 12	20, 70, 2, 12
$I_D$ curve form $I_{D,max}$	As in Figure 2 105 A	As in Figure 2 and 4 105 A	As in Figure 2 450 A
$T_e(z_2)$ $T_e$ scale length	6.18 eV (Fig 2) 0.0172 m (Figure 2)	3.5-5 eV (Fig 4) 0.0172 m	6.18 eV (Fig 2) 0.0172 m
$n_e(z_2)$ at $I_{D,max}$ $n_e$ scale length	$10^{19} \text{ m}^{-3}$ (Figure 2) 0.0195 m (Figure 2)	$0 - 3 \times 10^{19} \text{ m}^{-3}$ (Figure 4) 0.0195 m	$4.5 \times 10^{19} \text{ m}^{-3}$ 0.0195 m
$\omega_{ge} \tau_c$ (giving $\eta_{\perp}$ )	2 (HIPIMS value)	1 - 50	2 (HIPIMS value)

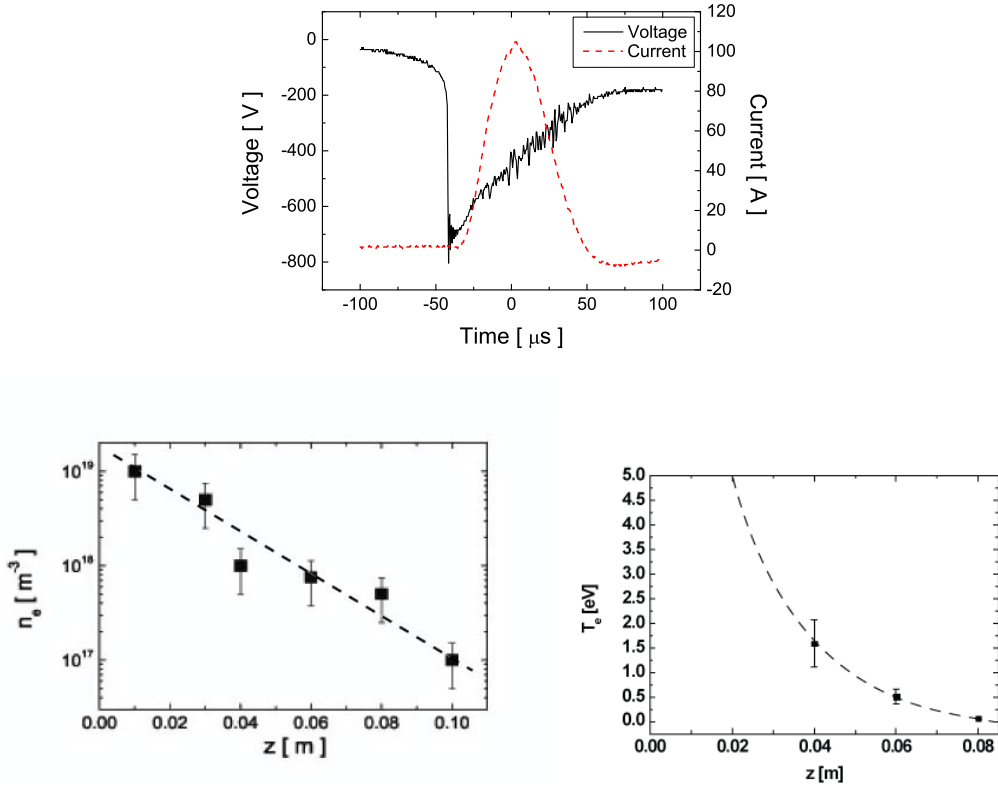


Figure 2. The experimental parameters from Lundin et al [7]. Top: discharge current and voltage. Bottom: The values of density and electron temperature above the racetrack at current maximum: measurements with error bars, and analytical fits shown with dashed lines.

The cross- $\mathbf{B}$  resistivity  $\eta_{\perp}$  in Eq:s (2.1) and (2.2) determines the electron drift speed in response both to electric fields and pressure gradients, *i.e.*, the electric conductivity and the electron diffusion coefficient, respectively, as discussed in Appendix B. The resistivity is known in both dc [5] and HIPIMS [6] magnetrons to depart from the classical values that are derived from electron-neutral and Coulomb collisions. The determination of the effective electron collision time  $\tau_c(r_c, z, t)$  has been one of the key tasks in the experimental investigations [7, 8]. It gives an anomalous transverse resistivity that can be written as a function  $\eta_{\perp}(\tau_c, B, n_e)$  and which is used as an input parameter in the BPM model,

$$\eta_{\perp} = \frac{m_e}{\tau_c e^2 n_e} = \frac{B}{\omega_{ge} \tau_c e n_e}, \quad (2.3)$$

where the last step is made using the electron angular gyro frequency  $\omega_{ge} = eB/m_e$ . In dc magnetrons,  $\omega_{ge} \tau_c$  lies in the range  $8 < \omega_{ge} \tau_c < 30$  [5,11], which is often referred to as the Bohm regime. In pulsed magnetrons recent measurements in different devices [6,7,12] agree on a value around  $\omega_{ge} \tau_c = 2$ .

### 3. Calculations

#### 3.1. Potentials with HIPIMS resistivity

Figure 3 shows calculated potentials from run 1 of the bulk plasma model which uses the experimental density and temperature profiles of Figure 2 at current maximum, and the resistivity  $\eta_{\perp}$  of Eq. (2.3) with  $\omega_{ge} \tau_c = 2$  for a HIPIMS discharge. The left hand panel shows the potential in the  $(r_c, z)$  plane, and the panel to the right shows the profile above the racetrack centre. Most important for the ion motion is a region of electric field reversal above the racetrack that extends from the ionization region at  $z = z_2$  to  $z = 0.04$  m. The reversed field is strongest close to the ionization region at  $z_2$ , where  $E_z = 375 \text{ Vm}^{-1}$ . We have, from the intermediate steps of the model calculations, extracted (but do not show here) the pressure-driven contribution (from Eq. (2.1)) and the electric-field driven contribution (from Eq. (2.2)) to the discharge current density. The field reversal happens on magnetic flux surfaces across which the pressure-driven part of the current would be larger than the discharge current itself. The explanation for the electric field reversal is therefore the same as for analogous field reversals in glow discharges, low voltage arcs, etc. [13]: when the electron pressure falls steeply in the direction opposite to that of the external field, the total field may be completely suppressed or even reverse in direction with respect

## A bulk plasma model for magnetrons

to the current. Such a reversed field has positive consequences for the deposition yield of the ionized component. Even the ions with lowest energy that come out from the ionization region (shaded in Figure 3) will be accelerated outwards and not be drawn back to the target. Of those that become ionized outside the ionization region only a small minority, those ionized around the minimum at  $z = 0.04$  m and with energies below 1 eV, might have trouble to overcome the weak electric field at  $z > 0.04$  m and reach the substrate.

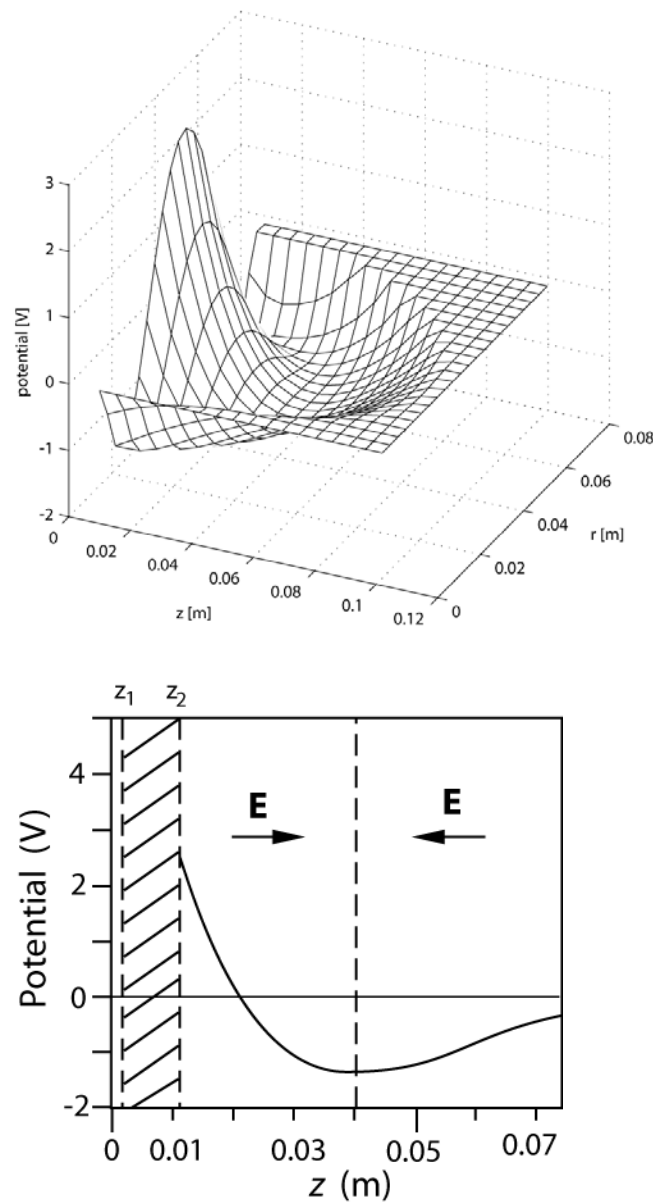


Figure 3. Top: the potential at current maximum of model run 1, with HIPIMS resistivity and with experimental electron density and electron temperature. Bottom: the potential as function of  $z$  above the middle of the racetrack. The shaded region between  $z_1$  and  $z_2$  shows the ionization region in which the potential is unknown.

## A bulk plasma model for magnetrons

Figure 4 shows the time variation of the potential, above the racetrack centre, during a current pulse. The top panel shows the input data: the discharge current  $I_D(t)$ , and the calculated  $n_e(z_2, r_{crt}, t)$  and  $T_e(z_2, r_{crt}, t)$  from the ionization region model. In spite of large variations of both discharge current and plasma density, the potential profile in Figure 4 remains essentially the same during the whole pulse: a field reversal in the region  $z_2 < z < 0.04$  m, and a bulk plasma potential that nowhere departs more than a few volts from ground potential.

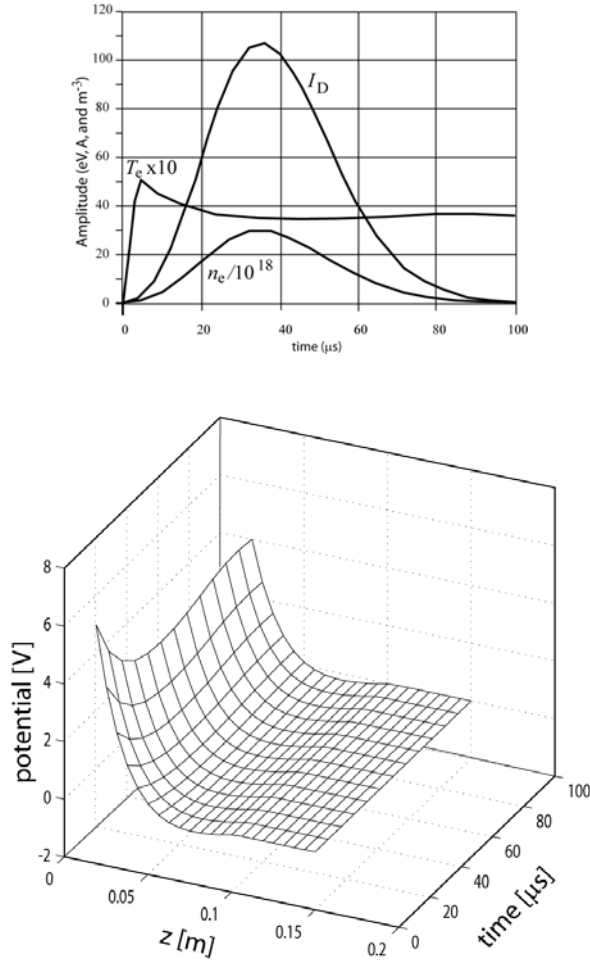


Figure 4. Model run 2, with  $\omega_{ge}\tau_c = 2$ . The top panel shows the discharge current (which is the same as in the experiment, Fig. 2), and the time variation of the plasma density  $n_e(t)$ , and the temperature  $T_e(t)$  at ( $z = z_2, r_c = r_{rc}$ ), taken from the ionization region model [9]. The bottom panel shows the potential above the racetrack centre for  $z > z_2$ , as function of  $t$ .

### 3.2. Dependence of potentials on the resistivity

Figure 5, left panel, shows the plasma potential above the racetrack obtained for model run 2, at current maximum, for a range of  $\omega_{ge}\tau_c$  from 1 to 50. The potential profile  $U_p(z)$  for the value  $\omega_{ge}\tau_c = 2$  corresponds to the curve at 35  $\mu\text{s}$  in Fig 4. The right panel of Figure 5 shows measured potentials over the racetrack in a dc magnetron [5]. From measurements of the current density ratio  $J_H/J_D$ , it was in [5] estimated that  $\omega_{ge}\tau_c \approx 7.7 \pm 4.2$ . Inlaid dashed lines and error bars show the corresponding potential from the model *i.e.*,  $\omega_{ge}\tau_c = 8 \pm 4$  from the left panel. In spite of the fact that these are two different machines run at quite different power, there is good agreement. Notice also that there is only a small spread in the experimental data of Bradley *et al* [5], in spite of large variations of power, 10 – 150 W, and in neutral pressure, 0.26 - 0.65 Pa. Altogether, the data in Figure 5 indicates that the resistivity  $\eta_{\perp}$  (properly normalized by the value of  $\omega_{ge}\tau_c$ ) is the most important single parameter to determine the potential profile. The good agreement between model and experimental data, in the right hand panel, also serves to bench-mark the bulk plasma model in the dc magnetron regime.

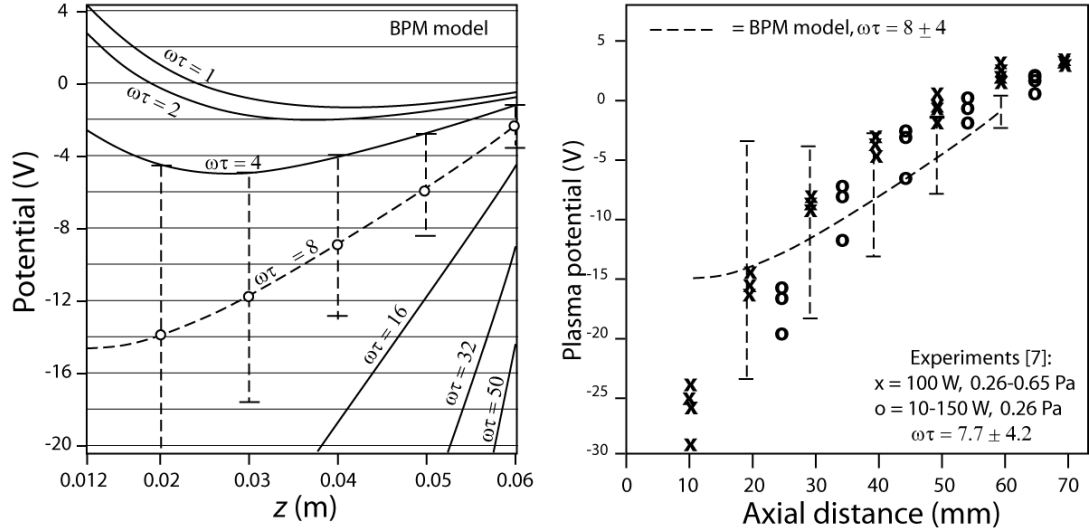


Figure 5. Left panel: potentials above the racetrack for model run 2, at current maximum but with  $\omega_{ge}\tau_c$  varied. Right panel: measurement of Bradley *et al*, [5]. The inlaid dashed lines show the model calculation, from the left panel, for  $\omega_{ge}\tau_c = 8 \pm 4$ .

### 3.3. Current densities with HIPIMS resistivity

A corresponding comparison cannot be made in the HIPIMS magnetron regime because there are yet no measurements of the potentials. For bench-marking against HIPIMS magnetron data we have therefore run the model with parameters corresponding to the 300 kW experiment by Böhlmark *et al* [6], where the azimuthal current densities were measured. This is model run 3 in Table I. This discharge had roughly the same voltage and current curve forms as the 50 kW discharge of Lundin *et al* [7] shown in Figure 2, but a factor 4.5 higher plasma density and discharge current. We use the HIPIMS value  $\omega_{ge}\tau_c \approx 2$  which was actually experimentally determined in this experiment [6]. The top panel in Figure 6 shows the calculated azimuthal current density at the discharge current maximum, and the bottom panel shows the experimental results from [6] with the model current density contours at  $J_\phi = 10, 20, 30, 50,$  and  $70 \text{ kA m}^{-2}$  inlaid as dashed lines. There is fair agreement regarding both the shapes of the constant-current-density contours, and the absolute values. The electric fields and potentials (not shown) obtained for this 300 kW discharge are very similar to those in the 50 kW discharge shown in Fig 3, again supporting our conclusion that  $\omega_{ge}\tau_c$  is the key parameter for the electric field strength and the potential profile.

The nature of the azimuthal current  $\mathbf{J}_\phi$  has earlier been discussed in the literature. In a dc magnetron Bradley *et al* [5] found that it is dominated by the Hall drift  $\mathbf{u}_e = \mathbf{E} \times \mathbf{B} / B^2$  of the electrons throughout the plasma volume, but in some regions with minor contribution from the  $\nabla B$  and curvature drifts. In a pulsed dc magnetron [11], it was found that during the ‘on’ phase  $\mathbf{J}_\phi$  was carried mainly by Hall drifting electrons, while some other mechanism kept  $\mathbf{J}_\phi$  remaining for some time also in the ‘reverse’ phase. In the high power densities of HIPIMS magnetrons, Böhlmark *et al* [6] and later Lundin *et al* [7] have argued that the diamagnetic (electron-pressure driven) electron drift can give quite significant contributions to  $\mathbf{J}_\phi$ .

In our model calculations we find the following patterns. In the dc magnetron case, corresponding to a range of  $8 < \omega_{ge}\tau_c < 30$  of model run 2, the Hall drift indeed gives the dominating contribution to  $\mathbf{J}_\phi$  throughout the plasma except for the combination of the lowest value of  $\omega_{ge}\tau_c$  with the region closest to the racetrack, about  $z \leq 0.03 \text{ m}$ . Here also the diamagnetic contribution to the current is significant. In the HIPIMS runs (n:o 1

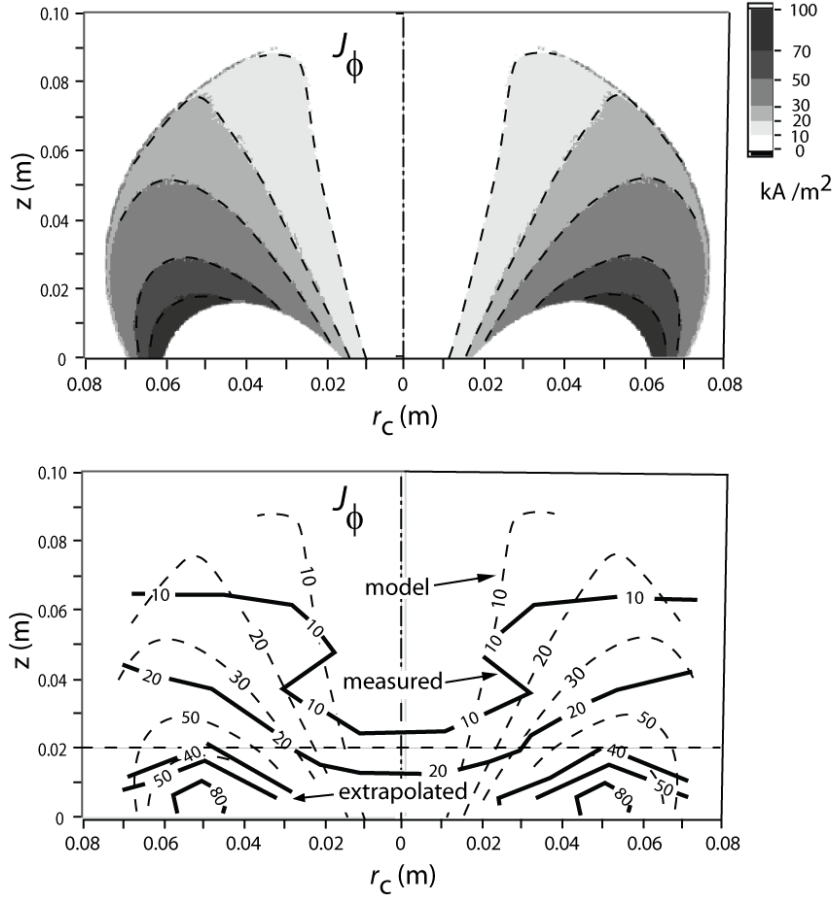


Figure 6. Top: the modelled azimuthal current density from model run 3 at current maximum. Bottom: the measurements by [6] with the model results added as dashed lines.

and 3 in Table I) with  $\omega_{ge} \tau_c = 2$ , there is a change at the magnetic flux surface that passes through the potential minimum (see Fig 3). Exactly at this surface  $\mathbf{E} = 0$ , the electron Hall drift is zero, and  $\mathbf{J}_\phi$  is completely a diamagnetic current. For increasing distance outside this surface, the Hall drift gives an increasingly large contribution to  $\mathbf{J}_\phi$ , and the diamagnetic part decreases accordingly. Inside the limiting surface however, the sign of the Hall drift is reversed. The diamagnetic contribution to  $\mathbf{J}_\phi$  is actually larger than the azimuthal current, but it is in this region counteracted by a weaker Hall current with the opposite sign. (We note for clarity that this reversal of the sign of the Hall current never gives a reversal of the total  $\mathbf{J}_\phi$  current which always runs in the usual direction).

#### 4. Summary and discussion

A plasma discharge model has been developed for the bulk plasma in sputtering magnetrons, also called the extended presheath. It can be used both for HIPIMS and dc sputtering magnetrons. New insight is obtained in the structure and time development of the currents, the electric fields, and the potential profiles. New findings are that in the HIPIMS mode, as a consequence of a high value of  $\eta_{\perp}$ : (1) There is an electric field reversal in a region extending in our case 0.01-0.04 m above the target, implying that there must be a potential maximum somewhere between 0.01 m and the target surface. (2) The electric field in the bulk plasma is typically an order of magnitude weaker than in dc magnetrons. (3) In the region closest to the target, the azimuthal current is diamagnetic in nature rather than being a Hall current.

These results are relatively insensitive to variations in discharge current, plasma density, and electron temperature. They are important for the ion transport in the bulk plasma through two mechanisms to be discussed below: (1) quasi-dc electric fields, on the time scale of the discharge pulse, that need to be maintained by the external circuit in order to drive the discharge current, and (2) forces in the azimuthal direction, which can be obtained from the azimuthal current densities calculated in the model.

*(1) Influence of quasi-dc E fields.* In Figure 5 both the experimental data [5] and the model calculations (with  $\omega_{ge}\tau_c \approx 8$ ) agree that the electric field in dc magnetrons is everywhere directed towards the target, and that the potentials involved are large enough to completely hinder the escape of  $M^+$  ions at a typical sputtering energy of 5 eV. This is different in the HIPIMS case, as shown in figures 3 and 4. Ions should, in these potential profiles, at no time during the pulse have trouble to reach the substrate once they have come outside the potential maximum in the ionization region. The forward-directed electric field, extending out to 0.04 m from the target, would actually hinder ions to return to the target even if they become directed that way after collisions. The reason for the reduced deposition rate in HIPIMS mode must be sought elsewhere.

*(2) Forces in the azimuthal direction.* The azimuthal current gives an azimuthal drag force on the ions due to resistive electron-ion friction. An estimate of this force was made based on experimental HIPIMS data in [8] for the location where the current is strongest, at  $z = 0.01$  m above the racetrack centre. The conclusion was that the ions can get an average azimuthal acceleration corresponding to typically 10 eV. This gives a sideways deflection, away from the substrate, that was experimentally verified by a 20 - 25 % (normalized)

## A bulk plasma model for magnetrons

increased deposition rate on the sides of the device. Using the model output, the azimuthal drag can be studied in much more detail. The time- and space resolved volume force on the ions can be expressed (see appendix A) in two equivalent ways

$$\mathbf{F}_{i\varphi} = -en_e\eta_{\perp}\mathbf{J}_{\varphi} = -\frac{B\mathbf{J}_{\varphi}}{\omega_{ge}\tau_c} \quad (4.1)$$

where the last step was made using Eq. (2.3). All quantities needed for either of these two forms is available explicitly in the model. Dividing the volume force with the plasma density (that is also in the model) gives the force per ion. This, together with the electric fields and potentials, can be used to follow the motion of ionized metal ions  $M^+$  in the bulk plasma.

Although the benchmarking against experiments in Figures 5 and 6 is encouraging, more direct comparisons to experiments would be valuable, in particular measurements of the plasma potential in the HIPIMS mode. Such measurements are however difficult to make. Floating probe potentials suffer large offsets [19] due to the variations in electron temperature, while emitting probes would have short lifetimes due to the high emission currents needed in the dense HIPIMS plasmas. A possibility is baffled probes [20] for which the floating potential is less sensitive to electron temperature. Another key experimental issue is to obtain better estimates of the model parameter  $\omega_{ge}\tau_c$  that determines the resistivity  $\eta_{\perp}$  through Eq. (2.3). The estimates made so far in HIPIMS devices rely on electron drift speed estimates [7] or on current density ratios  $J_{\varphi}/J_D$  from global magnetic measurements [6], both with limited time and space resolution. To improve this situation, we are developing current-density probes that can give space and time resolved  $J_{\varphi}$  and  $J_D$ .

Future work also involves combining the ionization region model [9] and the present bulk plasma model into one unified model, in which sputtered atoms can be regarded as test particles. They can then be followed from the target in a Monte Carlo simulation through regions with known plasma density and electron temperature. Their points of ionization, and their subsequent motion under the action of the electric and the current friction forces, can then be studied. The goal of such a project would be to identify the regimes of operation that give the best combination of high deposition rate and high degree of ionization. Another important topic for future work is the potential profile  $U(z)$ , both inside the ionization region ( $z < z_2$ ) where there must be a potential maximum, and in the

bulk plasma ( $z > z_2$ ) for other values than  $z_2 = 0.012$  m which has been used throughout this paper.

### Acknowledgements

This work has been partly supported by the European Commission within the 6<sup>th</sup> framework (integrated project InnovaTiAl), and the Swedish Research Council.

### Appendix A. Calculation procedure

The input files for the three model runs are listed in Table I. In the present calculation we assume that the  $\mathbf{B}$ -parallel components of the electron temperature gradient, and also the volume forces on the electrons, are zero:  $\mathbf{E} \cdot \mathbf{B} = 0$ ,  $\nabla T_e \cdot \mathbf{B} = 0$ , and  $\nabla p_e \cdot \mathbf{B} = 0$ . Values of  $n_e$ ,  $T_e$ , and the plasma potential  $U_p$  are then constant on field lines and can therefore be found from those above the racetrack centre. (Errors introduced by this assumption is a probable reason for the remaining discrepancies between the calculated and the experimental azimuthal current densities in Figure 6). The current densities, the electric fields, and the potentials are then all calculated using the Generalized Ohm's Law [10]. In the rest frame of the ions, which in the bulk plasma we take as a good approximation of the lab rest frame, the  $\mathbf{v} \times \mathbf{B}$  term disappears and the equation becomes

$$\frac{m_e}{e^2 n_e} \frac{d\mathbf{J}}{dt} + \eta \mathbf{J} + \frac{\mathbf{J} \times \mathbf{B}}{en_e} = \mathbf{E} + \frac{\nabla p_e}{en_e}. \quad (5.1)$$

With typical numbers (discharge time scale  $10^{-5}$  s, and  $B \approx 10^{-2}$  T) the first term is four orders of magnitude smaller than the third and can also be neglected. Solving separately for the two terms on the right hand side gives two equations, Eq. (2.1) for the pressure-driven part  $\mathbf{J}_{\nabla p_e}$  of the current density, and (2.2) for the part  $\mathbf{J}_E$  of the current density that is driven by the electric field. For each of these, we calculate the current across magnetic flux surfaces obtained by rotation around the symmetry axis of field lines that intersect the cathode (= the target) at both ends. Since the discharge current  $I_D$  has to equal the integrated perpendicular current across each such surface, we need not keep track of the field-aligned current and can replace  $\eta$  (which actually is a tensor) with the cross- $\mathbf{B}$  resistivity  $\eta_{\perp}$  of Eq. (2.3). Also, the azimuthal currents do not contribute to the discharge current. For the discharge current we need therefore calculate only the current densities perpendicular to the magnetic flux surfaces. We denote them below by index  $D$  for Discharge:  $\mathbf{J}_{D\nabla p_e}(z, r_c)$  and  $\mathbf{J}_{DE}(z, r_c)$ . The calculations are for each time  $t$  made in five successive steps:

(1) The pressure-gradient-driven contribution to the discharge current density

$\mathbf{J}_{D\nabla p_e}(z, r_c)$  is calculated using Eq. (2.1), in steps of 0.1 mm along each field line down to the distance  $z_1$  from the target surface.

(2) The pressure-driven total current  $I_{D\nabla p_e}$  is calculated across 1500 about equally spaced flux surfaces, defined by rotation of these magnetic field lines around the symmetry axis, and integrating the  $\mathbf{J}_{D\nabla p_e}(z, r_c)$  values from step 1.

(3) The electric field  $\mathbf{E}(z, r_c)$  is the field strength needed to give a divergence-free total current across the flux surfaces, equal to the discharge current  $I_D$ . It is calculated using the input file  $I_D(t)$  combined with Eq. (2.2) and the  $I_{D\nabla p_e}$  data from step (2). This procedure also gives the E-field driven discharge current density array  $\mathbf{J}_{DE}(z, r_c)$ .

(4) The plasma potential  $U_p(z, r_c)$  is calculated by integration of  $\mathbf{E}(z, r_c)$  from an assumed ground potential far from the target.

(5) From the data arrays created above, simple addition gives the arrays of total discharge current density  $\mathbf{J}_D(z, r_c) = \mathbf{J}_{D\nabla p_e}(z, r_c) + \mathbf{J}_{DE}(z, r_c)$ , and the azimuthal current density  $\mathbf{J}_\varphi(z, r_c) = \omega_{ge} \tau_c \mathbf{J}_D(z, r_c)$ .

## Appendix B. Conductivity, resistivity, and diffusion

The origin of the high resistivity in the HIPIMS magnetron at LiU is discussed in [7,14]. The azimuthal current  $\mathbf{J}_\varphi$  corresponds to azimuthal ion-electron drift velocities well above both the typical speed of a 5 eV sputtered particle and the ion acoustic speed of  $\text{Ar}^+$  ions. The current therefore is two-stream (cross- $\mathbf{B}$ ) unstable and drives either the modified two-stream instability MTSI, the lower hybrid drift instability, or a mixture of both [15]. The fine structure inside this class of instabilities is known both from simulations [16,17], and from measurements in another type of plasma device operated in the same parameter regime as ours [17]. The dominating frequency is in the lower hybrid range, and the density variations and (wave) electric fields are strongly correlated. Due to this correlation, the waves give a net force  $\mathbf{F}_{ei} = \langle -e\mathbf{E}_{w,\varphi} n_e \rangle = -en_e \eta_\perp \mathbf{J}_\varphi$  between ions and electrons, directed along the current  $\mathbf{J}_\varphi$ . This corresponds to a macroscopic transverse resistivity given by the average of the force over the wave structure,  $\eta_\perp = \langle n_e E_\varphi \rangle / J_\varphi \langle n_e \rangle$ . Through the Generalized Ohm's Law, Eq. (5.1) below, the resistivity determines all electron motion across  $\mathbf{B}$ : the Hall and Pedersen currents that are driven by electric fields, and also the

diamagnetic current and the diffusion flux that are driven by electron pressure gradients. For the electron flux components in the directions of the electric field and the electron pressure gradient, Eq. (2.1) corresponds to diffusion and Eq. (2.2) to electric conduction with Pedersen conductivity. The effective time of electron momentum transfer to the ions, often called the effective electron collision time  $\tau_c$ , is related [18] to the resistivity  $\eta_{\perp}$  through Eq. (2.3). The dimensionless product  $\omega_{ge}\tau_c$  that appears in Eq. (2.3) can be seen as a normalization of  $\tau_c$  to the gyro time scale  $\omega_{ge}^{-1}$ . Similar values of  $\omega_{ge}\tau_c$  enable a scaling through Eq. (2.3) of the resistivity between devices with widely different values of magnetic field strength and plasma density [14]. In the bulk plasma of magnetrons, where the current is carried mainly by the electrons,  $\omega_{ge}\tau_c$  can be directly obtained from a macroscopic measurement of the current density ratio as  $\omega_{ge}\tau_c = J_{\phi} / J_D$  [5, 8,10].

## References

- [1] Kouznetsov V, Macák K, Schneider J M, Helmersson U, and Petrov I, *Surf. Coat. Technol.* **122**, 290, 1999
- [2] Helmersson U, Latteman M, Böhlmark J, Ehiasaran A P, and Gudmundsson J T, Ionized physical vapor deposition (IPVD): a review of technology and applications, *Thin Solid Films*, Vol **513**, p. 1-24, 2006
- [3] Ehiasarian A P, New R, Munz W D, Hultman L, Helmersson U, and Kouznetsov, V, *Vacuum* **65**, 147, 2002.
- [4] Böhlmark J, Lattemann M, Gudmundsson J T, Ehiasarian A P, Aranda Gonzalvo Y, Brenning N, and Helmersson U, The ion energy distributions and ion flux composition from a high power impulse magnetron sputtering discharge, *Thin Solid Films*, **515**, 1522, 2006.
- [5] Bradley J W, Thompson S, and Gonzalvo Y A, Measurements of the plasma potential in a magnetron discharge and the prediction of the electron drift speeds, *Plasma Sources Sci. Technol.* **10**, 490-501, 2001.
- [6] Böhlmark J, Helmersson U, VanZeeland M, Axnäs I, Alami J, and Brenning N, Measurements of the magnetic field change in a pulsed high current magnetron discharge, *Plasma Sources Sci. Technol.* **13**, 645-661, 2004.
- [7] Lundin D, Helmersson U, Kirkpatrick S, Rohde S, and Brenning N, Anomalous electron transport in high power impulse magnetron sputtering, *Plasma Sources Sci. Technol.* **17** (2008) 000000 (9pp).

- [8] Lundin D, Larsson P, Wallin E, Lattemann M, Helmersson U, and Brenning N, Cross-field ion transport during high-power impulse magnetron sputtering, Manuscript in preparation for *Plasma Sources Sci. Technol.*, 2008.
- [9] Raadu M A, Axnäs I, Gudmundsson J T, and Brenning N, An ionization region model for HIPIMS magnetrons, *Manuscript in preparation for Plasma Sources Sci. Technol.*, 2008.
- [10] Spitzer L, *Physics of Fully Ionized Gases*, Interscience Publishers, John Wiley & Sons, 1962
- [11] Rossnagel S M, and Kauffmann H R J, Induced drift currents in a circular planar magnetron, *Vac. Sci Technol.* **A5**, 2276, 1987
- [12] Vetushka A, and Bradley J E, 2007, The current-density distribution in a pulsed magnetron deposition discharge, *J. Phys. D: App. Phys.* **40**, pp 2037-2044
- [13] Raizer Y P, *Gas Discharge Physics*, Springer-Verlag Berlin Heidelberg, page 31, 1991.
- [14] Brenning N, Lundin D, Merlino R, and Helmersson U, 2008. Anomalous transverse resistivity corresponding to  $\omega\tau = 2$  in pulsed plasmas that are driven electrically, magnetically, or kinetically, Manuscript in preparation.
- [15] Hsia J B, Chiu S M, Hsia M F, Chou R L, and Wu C S, Generalized lower-hybrid-drift instability, *Phys. Fluids*, Vol **22**, Issue 9, pp 1737-1746, 1979.
- [16] Machida S, Abe T, and Terasawa T, Computer simulation of Critical Velocity Ionization, *Phys. Fluids* **27**, 1928, 1984.
- [17] Hurtig T, Brenning N, and Raadu M A, The role of high frequency oscillations in the penetration of plasma clouds across magnetic boundaries, *Phys Plasmas* **12**, 012308, 2005
- [18] Chen F, *Introduction to Plasma Physics and Controlled Fusion, Vol 1, second edition*, Plenum Press, New York, p. 180, 1984.
- [19] Hutchinson I H, *Principles of Plasma Diagnostics*, Cambridge University Press, Cambridge New York Sydney, page 64, 1987.
- [20] Demidov V I, Finnegan S M, Koepke M E, and Reynolds E W, Baffled probe for real-time measurements of space potential in magnetized plasmas, *Rev. Sci. Instr.* Vol **74**, No **10**, 4558, 2003.